

Detection of Microcalcifications in Digital Mammograms Using Wavelets

Ted C. Wang and Nicolaos B. Karayiannis,* *Member, IEEE*

Abstract—This paper presents an approach for detecting microcalcifications in digital mammograms employing wavelet-based subband image decomposition. The microcalcifications appear in small clusters of few pixels with relatively high intensity compared with their neighboring pixels. These image features can be preserved by a detection system that employs a suitable image transform which can localize the signal characteristics in the original and the transform domain. Given that the microcalcifications correspond to high-frequency components of the image spectrum, detection of microcalcifications is achieved by decomposing the mammograms into different frequency subbands, suppressing the low-frequency subband, and, finally, reconstructing the mammogram from the subbands containing only high frequencies. Preliminary experiments indicate that further studies are needed to investigate the potential of wavelet-based subband image decomposition as a tool for detecting microcalcifications in digital mammograms.

Index Terms—Breast cancer screening, digital mammography, microcalcification detection, wavelet image decomposition.

I. INTRODUCTION

SCREEN-FILM mammography is widely recognized as being the only effective imaging modality for early detection of breast cancer in women. Screening asymptomatic women using screen-film mammography has been shown to significantly reduce breast cancer mortality [21]. Medical doctors generally examine the breast radiographs for the presence of malignant masses and indirect signs of malignancy, such as the presence of microcalcifications and skin thickening. Thus, the imaging performance achieved by screen-film radiography is very important.

During the past 20 years, there have been many significant technological improvements in mammographic X-ray equipment and in screen-film processing systems [1]. Even though advances in screen-film mammographical technology have resulted in significant improvements in image resolution and film contrast, images provided by screen-film mammography remain very difficult to interpret. Moreover, technical advances in screen-film mammography are unlikely to provide good visualization in regions of interest to medical doctors. The minor difference in X-ray attenuation between normal

glandular tissues and malignant disease results in poor visualization in analog films [11]. This problem is accentuated when examining for breast cancer younger women who have denser breast tissues. Although microcalcifications have high inherent attenuation properties, their small size also results in a low subject contrast [30]. As a result, the visibility of small tumors, and any associated microcalcifications, will always be a problem in screen-film mammography.

Mammograms are among the most difficult of radiological images to interpret. Mammograms are of low contrast, and features in mammograms indicative of breast disease, such as the microcalcifications, are often very small. The large amount of negative biopsies encountered in current practice could be reduced if a computer system was available to help the radiologists to prescreen mammograms. With the advent of high-resolution image digitization hardware, the decreasing cost/performance ratio of computers, and the recent development of digital X-ray image acquisition equipment, computer-aided image analysis is becoming practical for mammograms.

This paper proposes a system designed to perform prescreening of digital mammograms for the presence of microcalcifications based on their wavelet decomposition. This paper is organized as follows: Section II presents a review of existing techniques for mammographical feature analysis. Section III presents the mathematical foundation of wavelet analysis and filter banks theory. Section IV describes the structure of the system proposed for microcalcification detection and presents an example of the system in operation. Section V includes concluding remarks and proposes some directions for future work.

II. ENHANCEMENT AND DETECTION OF MAMMOGRAPHIC FEATURES

This section reviews image enhancement techniques for digital mammograms and approaches attempting to detect, extract, and segment clustered microcalcifications.

A. Enhancement of Mammograms

The fundamental enhancement needed in mammography is an increase in contrast, especially for dense breasts. Contrast between malignant tissue and normal dense tissue may be present on a mammogram but below the threshold of human perception. Similarly, microcalcifications in a sufficiently dense mass may not be readily visible because of low contrast

Manuscript received October 9, 1996; revised July 27, 1998. The Associate Editor responsible for coordinating the review of this paper and recommending its publication was M. W. Vannier. *Asterisk indicates corresponding author.*

T. C. Wang is with PCD R & D, U.S. Robotics, Skokie, IL 60077-2690 USA.

*N. B. Karayiannis is with the Department of Electrical and Computer Engineering, University of Houston, Houston, TX 77204-4793 USA (e-mail: karayiannis@uh.edu).

Publisher Item Identifier S 0278-0062(98)08580-2.

[30]. As a result, defining the characteristics of microcalcifications is difficult.

Conventional image processing techniques do not perform well on mammographic images. The large variation in feature size and shape reduces the effectiveness of classical fixed-neighborhood techniques such as unsharp masking [18]. Fixed-neighborhood or global techniques may adapt to local features within a neighborhood, but do not adapt the size of the neighborhood to local properties. Alternatively, they modify the image depending on global properties, such as the image spatial-frequency spectrum, which may not be representative of a small region of interest in the image. Many images, including mammograms, have isolated regions which are the primary feature of interest. These features can vary widely in size and shape, and often cannot be enhanced by fixed-neighborhood or global techniques. There are two possible approaches to enhancing mammographic features. One is to increase the contrast of suspicious areas as stated earlier, and the other is to remove background noise.

Morrow *et al.* [18] used a “region-based image processing” technique which adapts to image features and enhances these features with respect to their surroundings, regardless of the shape and size of the features. In adaptive-neighborhood or region-based image processing, a neighborhood is defined about each pixel in the image, the extent of which is dependent on the characteristics of the image feature in which the given pixel is situated. This neighborhood of similar pixels is called a *region*. If properly defined, regions should correspond to image features. Then, image processing procedures can be applied on an image feature basis, rather than pixel by pixel. There are two classes of regions: nonoverlapping regions, which are obtained using image segmentation techniques, and overlapping regions, obtained using region grouping techniques. Morrow *et al.* considered overlapping regions, because they felt that disjoint segmentation of an image with subsequent enhancement of the segments would result in noticeable edge artifacts and an inferior enhanced image. Their method uses each pixel in the image as a seed to grow a region. The extent and shape of the region adapt to local image gray-level variations, corresponding to an image feature. The contrast of each region is calculated with respect to its individual background. Contrast is then enhanced by applying an empirical transformation based on the seed pixel value of each region, its contrast, and its background. The objective of this scheme is to enhance the quality of “difficult” mammograms to allow the radiologists to make their diagnosis with more confidence. In order to achieve this objective, Morrow *et al.* used high-resolution digitization (less than 0.1-mm square pixel size), and maintained high resolution throughout their processing procedures.

Some researchers attempted contrast enhancement of mammographical features by utilizing the unique properties of frequency and orientation selectivity of the wavelet transform. Laine *et al.* [13] used three different multiscale representations: 1) the dyadic wavelet transform, 2) the ϕ -transform, and 3) the hexagonal wavelet transform. Each of these representations provides a hierarchy of multiscale images which localize important image information at different spatial frequencies.

Then they applied local and global nonlinear operators to this multiscale representation to enhance the desired features. More specifically, within each level of resolution they defined *multiscale edges* and used these edges as an “index” to increase the local gain of subband image coefficients in order to emphasize the desired mammographic features. They compared their results with traditional methods used for image enhancement such as unsharp masking and adaptive histogram equalization and found that the wavelet-based processing algorithms were superior [13].

An alternative to contrast enhancement of digital mammograms is the removal of background noise from these images. For instance, a digital mammogram can be enhanced by removing background noise while preserving the edge information of suspicious areas. This approach was investigated by Lai *et al.* [12], who used four selective averaging schemes and a modification of median filtering called *selective median filtering*. A selective median filter is defined as follows: Given a window $W(i, j)$, centered at image coordinates (i, j) , the output of the selective median filter is

$$\hat{x}_{i,j} = \text{median}\{x_{r,s} : (r, s) \in N(i, j), \text{ and } |x_{r,s} - x_{i,j}| < T\}$$

where $x_{i,j}$ is the image intensity at (i, j) , $N(i, j)$ is the area in the image covered by the window $W(i, j)$, and T is a threshold. In computing the median, the set of pixels is restricted to those with a difference in gray level no greater than some threshold T . The amount of edge smearing can be controlled by adjusting the parameter T . If T is small, the edge-preserving power of the filter is strong, but its smoothing effect is small. If T is large, the filter behaves the other way around.

B. Detection of Microcalcifications

Computer aided detection of microcalcifications in digital mammograms has been attempted by several researchers in the past. Dengler *et al.* [8] proposed an approach which uses a two-stage algorithm for spot detection and shape extraction. The first stage applies a weighted *difference of Gaussian* (DOG) filter for the noise-invariant and size-specific detection of spots, resulting in a DOG image. This DOG image represents the microcalcifications if a thresholding operation is applied to it. By performing morphological opening on the original image, the shape of the objects is preserved. Finally, the results of both filters are combined via a morphological reconstruction operation called *conditional thickening*. The topology and the number of the spots are determined by the first filter, while their shape is determined by the second filter.

Betal [3] also used mathematical morphology to extract microcalcifications from digital mammograms. In this approach, an enhancement algorithm was applied on a digitized mammogram to emphasize the edges and lines while smoothing homogeneous areas. In the second stage, a “top-hat” algorithm was applied to obtain unique markers for each microcalcification. This algorithm consists of three parts: iterative opening, subtraction, and thresholding. The threshold level was selected manually by a radiologist. The binary image produced by thresholding provided markers for the *morphological watershed algorithm*. Segmentation of the mi-

crocalcifications was achieved by applying the watershed algorithm. The final stage involved a numerical analysis of the detected microcalcifications. Information about microcalcification areas and boundary lengths give an indication of the spread of microcalcification sizes. Benign microcalcifications tend to be large structures (diameter >1 mm), while malignant microcalcifications tend to be smaller.

Nishikawa *et al.* [19] also developed a computerized technique to automatically detect clustered microcalcifications. Their method consists of three stages: First the signal-to-noise ratio of the microcalcifications is enhanced by filtering the image to reduce the normal background structure of the mammogram. Second, signals (potential microcalcifications) are identified by means of global gray-level thresholding, morphological erosion, and then a local adaptive gray-level thresholding. Third, the number of falsely detected signals are reduced by 1) examining the power spectrum of individual signals, 2) determining the spatial distribution of the signals, and 3) examining the relationship between size, shape and background pixel value of microcalcifications.

Cairns *et al.* [4] employed an algorithm involving several stages to achieve automated detection of clusters of microcalcifications. They first made the following assumptions to model microcalcifications in digital mammograms: microcalcifications are small in size, usually of linear or round shape, they are usually brighter than the neighboring pixels, their brightness value is relatively constant across their surface, and they have well-defined edges. Finally, they argued that microcalcifications become significant only if they occur in groups or clusters. Based on these assumptions, they used an algorithm involving the following stages: edge detection, contour hue generation, location of potential microcalcifications using graph searching, feature extraction, classification of the potential microcalcifications, and cluster detection. They were able to achieve a classification rate of 91.75% for single microcalcifications. They also achieved 100% true-positives with 0% false positives using the re-substitution method, and 98% true-positives with 0% false positives using the leave-one-out method for clustered microcalcifications.

Zhao *et al.* [31] developed a method for adaptively thresholding gray-level mammographical images. This approach combines morphological filtering operations with a rule-base. The objective of the authors is to extract the suspicious areas from a mammogram and provide location information on certain microcalcifications of predefined shapes and sizes to radiologists for further examination. They derived an adaptive threshold function from morphological operations. The following characteristic features of the microcalcifications were pertinent in deriving the adaptive threshold function: granular form, casting form, microcalcification size, and microcalcification density. The threshold set is controlled by the index numbers in the skeleton of shapes which represent microcalcifications in mammograms. The parameters of the adaptive threshold sets are obtained from interpreting umbra shadows from an image function. These steps can be summarized as follows: 1) preprocess a gray-level mammogram to smooth out background noise, 2) obtain the skeleton information of microcalcifications and determine the shadow size from

the skeleton using morphological operators, 3) select the thresholding value based on the size of microcalcifications, 4) classify the suspicious areas based on predefined shapes and sizes of microcalcifications, and reconstruct the gray levels around only the suspicious areas. Steps 3) and 4) need a rule-base that is provided by expert radiologists.

An observation from these studies on microcalcification detection is that local filtering techniques require the fine tuning of several parameters related to local image statistics and they frequently result in a large number of false positives. On the other hand, the application of morphological operators requires *a priori* knowledge of the resolution level of the mammograms in order to determine the size and shape of the structuring elements to be used. Besides manual adjustment of the detected areas, these techniques also tend to rely on many stages of heuristics attempting to eliminate false positives.

III. WAVELETS AND SUBBAND DECOMPOSITION

The theory of wavelets provides a common framework for numerous techniques developed independently for various signal and image processing applications. For example, multiresolution image processing, used in computer vision, subband coding, developed for speech and image compression, and wavelet series expansions, developed in applied mathematics, have been recently recognized as different views of a single theory. The classical approach for the analysis of *nonstationary* signals is the *short-time Fourier transform* (STFT) or Gabor transform. With the advent of *wavelet transform* (WT), short windows at high frequencies and long windows at low frequencies can be used to provide better signal resolution than the STFT.

Wavelet transform can also be seen from a *signal decomposition* view point. In this case, a signal is decomposed onto a set of basis functions which are called *wavelets* and are the core of wavelet analysis. These basis functions are obtained from a single *mother wavelet* by dilations and contractions (scalings), as well as translations or shifts. Hence, the concept of *scale* is essential in wavelet analysis (compared to the concept of frequency in Fourier analysis).

There are several types of wavelet transforms that can be chosen depending on the application. The *continuous wavelet transform* (CWT) can be used for continuous signals. In this case, both time and scale are continuous. The *discrete wavelet transform* (DWT) can also be defined for discrete signals. It is shown in this section that wavelet decomposition is closely related to multirate signal processing techniques. A particular wavelet decomposition relates to filter banks and can be the basis for subband coding schemes used in speech and image compression. In this section, we first explore the concepts of resolution and scale in CWT. Then we proceed to the discrete-time case, where we attempt to link DWT to filter banks and subband signal decomposition.

A. Why Use Wavelets?

In signal analysis, a signal $f(t)$ is often represented by a weighted sum of building blocks, or *basis functions*

$$f(t) = \sum_i c_i \psi_i(t) \quad (1)$$

where $\psi_i(t)$ are basis functions and c_i are coefficients or weights. Since the basis functions $\psi_i(t)$ are fixed, the information about the signal is carried by the coefficients. The simplest such representation uses translations of the impulse function as its only bases, yielding a representation that reveals information only about the time domain behavior of the signal. Choosing the sinusoids as the basis functions yields a Fourier representation that reveals information only about the frequency domain behavior of the signal. For the purpose of detecting spurious spikes, neither of the above representations is ideal. What we would like to have is a representation which contains information about both the time and frequency behavior of the signal. More specifically, we need to know the frequency content of the signal at a particular instant in time. However, resolution in time (Δt) and resolution in frequency ($\Delta \omega$) cannot both be made arbitrary small at the same time because their product is lower bounded by the inequality known as the *uncertainty principle* [2]

$$\Delta t \Delta \omega \geq 1/2. \quad (2)$$

This inequality means that we must tradeoff time resolution for frequency resolution, or vice versa. Thus, it is possible to get very good resolution in time if we are willing to settle for low resolution in frequency. Conversely, we can get very good resolution in frequency if we are willing to settle for low resolution in time. From a practical standpoint, low-frequency events are usually spread out in time (nonlocal), and high-frequency events are usually concentrated in time (localized). Thus, one way that we can obtain good time-frequency information from a signal is to design the basis functions to act like cascaded octave bandpass filters which repeatedly split the bandwidth of the signal in half.

To gain insight into the design of the basis functions that will properly convey information about a signal and at the same time satisfy the uncertainty principle, let us compare the impulse function and the sinusoids. The impulse function cannot provide information about the frequency behavior of a signal because it has an infinitesimally small support. On the other hand, the sinusoids cannot provide information about the time behavior of a signal because they have infinite support. What we seek, then, is a compromise between these two extremes: a set of basis functions $\{\psi_i\}$, each with finite support of a different width. The different support widths allow us to tradeoff time and frequency resolution in order to accurately examine different regions of a signal.

For a wavelet representation, the basis functions in $\{\psi_i\}$ are scaled and translated versions of the same prototype function $\psi(t)$, known as the *mother wavelet*. The scaling is accomplished by multiplying t by some scale factor; if we choose the scale factor to be a power of two, yielding $\psi(2^a t)$, $a \in \mathbb{Z}$, we get the cascaded octave bandpass filter we desire. Since ψ has finite support, it must be translated along the time axis in order to cover an entire signal. This translation is accomplished by considering all the integral shifts of ψ , that is, $\psi(2^a t - b)$, $b \in \mathbb{Z}$. Therefore, a signal can be represented

in wavelet domain, or a wavelet decomposition, as

$$f(t) = \sum_a \sum_b c_{ab} \psi_{ab}(t) \quad (3)$$

where $\psi_{ab}(t) = 2^{a/2} \psi(2^a t - b)$.

The coefficients c_{ab} can be computed via *wavelet transform*, whose implementation is closely related to a number of techniques used in signal processing. Driven by applications such as speech and image compression, a method called *subband coding* was first proposed by Crochiere *et al.* [5] in the late 1970's. This led to the study of perfect-reconstruction filter banks, a problem considered in the 1980's by several researchers including Smith and Barnwell [20], Mintzer [17], Vetterli [24], [25], and Vaidyanathan [22], [23]. In a particular configuration, namely when the filter bank has octave bands, one obtains a discrete-time wavelet series. Under certain conditions, such an octave-band filter bank can be used to generate wavelet bases.

Daubechies [6], [7] proposed one of the most interesting methodologies for wavelets. This methodology relies on the iteration of a discrete-time filter bank which, under certain conditions, converges to a continuous-time wavelet basis. Furthermore, the multiresolution framework used in the analysis of wavelet decompositions automatically associates a discrete-time perfect-reconstruction filter bank to any wavelet decomposition. The pyramid decomposition framework is central to wavelet decomposition and establishes conceptually the link between filter banks and wavelets, as shown by Mallat [14]–[16] and Daubechies [6], [7]. This connection has led to a renewed interest in filter banks, especially with the work of Daubechies who first constructed wavelets from filter banks [6] and Mallat who showed that a wavelet series expansion could be implemented with filter banks [14].

As can be seen from the above discussion, there are two different points of view about the advantages of wavelet representation and its implementation via filter banks. One is the expansion of signals in terms of a structured basis, and the other is the perfect reconstruction of signals via filter banks. While the two are equivalent, the former is more related to signal representation, while the latter is more concerned with the construction of implementable systems.

B. STFT: A Fixed-Resolution Analysis

The goal of signal analysis is to extract relevant information from a signal by transforming it. For a stationary signal $x(t)$ ¹ the natural “stationary transform” is the well-known Fourier transform

$$X(\omega) = \langle e^{j\omega t}, x(t) \rangle = \int_{-\infty}^{\infty} x(t) e^{-j\omega t} dt \quad (4)$$

which is also called the Fourier analysis formula. The inverse Fourier transform is given by

$$x(t) = \frac{1}{2\pi} \int_{-\infty}^{\infty} X(\omega) e^{j\omega t} d\omega \quad (5)$$

and is also called the Fourier synthesis formula. Note that $e^{j\omega t}$ is not in the space $L_2(\mathbb{R})$ of square integrable functions,

¹Mathematically, this also means an absolutely integrable function.

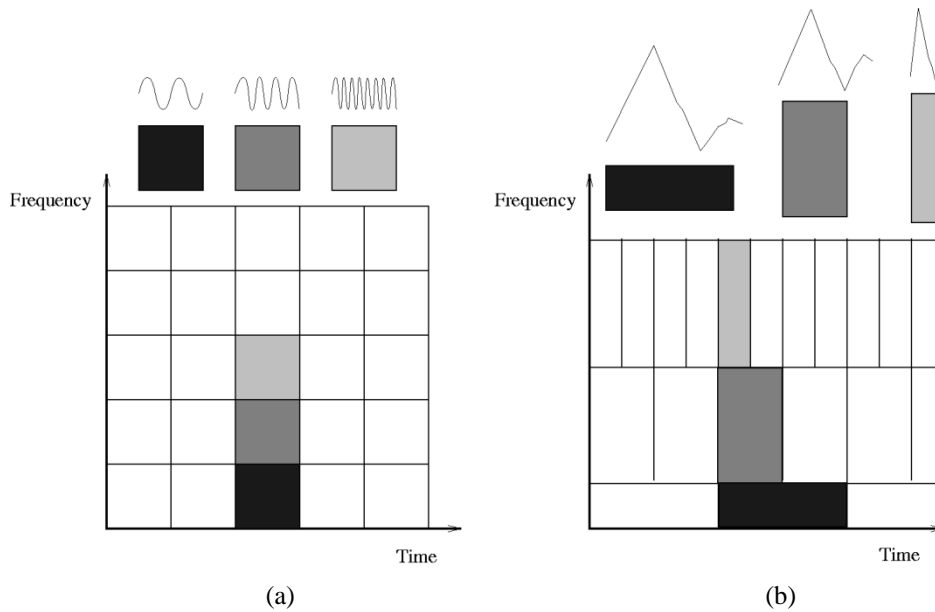


Fig. 1. Frequency tiling of (a) the STFT and (b) the WT and the corresponding basis functions. The tiles represent the concentration in time-frequency plane covered by a given basis function.

and that the set $\{e^{j\omega t}\}$ is not countable. As shown in (4), the Fourier coefficients $X(\omega)$ are computed as inner products of the signal $x(t)$ with sinusoidal basis functions of infinite duration. Consequently, Fourier analysis works well if $x(t)$ is composed of a few harmonic components. This implies that any abrupt change in time in a nonstationary signal $x(t)$ is spread out over the whole frequency axis in $X(\omega)$. Therefore, the analysis of nonstationary signals requires more than the Fourier transform.

To achieve a “local” Fourier transform, one can define a windowed Fourier transform. This modified version of the Fourier transform, called the STFT, was formulated by Gabor [10] to deal with nonstationary signals as

$$\text{STFT}(\tau, \omega) = \int x(t)g^*(t - \tau)e^{-j\omega t} dt \quad (6)$$

where $g^*(t)$ denotes the complex conjugate of the function $g(t)$. The STFT assumes the signal $x(t)$ to be stationary when seen through a window $g(t)$ of finite length, centered at time location τ . This modified transform can also be interpreted as a filtering process. The signal $x(t)$ is filtered with a bandpass filter having a frequency response equal to the windowing function $g(t)$, and then the Fourier transform is performed on this filtered signal.

The STFT can also be seen as a measure of similarity between the signal and a basis function, which is a shifted and modulated version of an elementary window, i.e.,

$$\text{STFT}(\tau, \omega) = \langle g_{\tau, \omega}(t), x(t) \rangle \quad (7)$$

where $g_{\tau, \omega}(t) = g(t - \tau)e^{j\omega t}$. Thus, each basis function used in the expansion has the same time and frequency resolution but occupies a different location in the time-frequency plane. Although the STFT seems to be the solution for nonstationary signals, it has a major drawback: poor time and frequency resolution. The analysis depends critically on the choice of

the window $g(t)$. Once this window is chosen, then the time-frequency resolution is *fixed* over the entire time-frequency plane since the same window is used at all frequencies. This situation is depicted in Fig. 1(a), which shows the frequency tiling of the STFT.

C. CWT: A Multiresolution Analysis

To overcome the resolution limitation of the STFT mentioned previously, one would like to be able to vary the frequency bandwidth and the time span of the analysis filter in order to achieve *multiresolution* analysis. More specifically, the time resolution must increase with the central frequency of the analysis filter, and the ratio of the filter bandwidth to its central frequency must be constant. This requirement corresponds to the so-called *constant-Q* analysis [25], [26]. In terms of filter banks, this means that instead of the frequency responses of the analysis filters being regularly spaced over the frequency axis (as for the STFT case), they are regularly spaced in a *logarithmic* scale.

When the constant relative bandwidth condition is met, the time resolution becomes arbitrarily good at high frequencies, while the frequency resolution becomes arbitrarily good at low frequencies. This enables the analysis of signals such as two very close short bursts, because by increasing the analysis frequency (higher time resolution) the two events can be well distinguished. This kind of multiresolution analysis works best if the signal under consideration has high-frequency components of short duration and low-frequency components of long duration. In fact, most images correspond to this type of signals.

Multiresolution analysis [14], [15] can be accomplished using the CWT. To define the CWT, we will not consider shifts and modulates of a prototype function as in STFT. Instead, we will use *scaled* and *shifted* versions from the same prototype to achieve the constant- Q condition. Consider a real bandpass

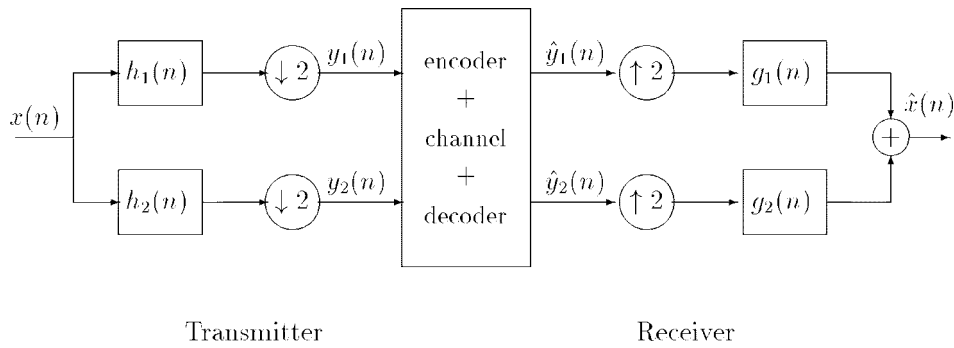


Fig. 2. Basic two-channel filter bank structure.

filter with impulse response $\psi(t)$ and zero mean

$$\int_{-\infty}^{\infty} \psi(t) dt = 0. \quad (8)$$

The CWT is defined as [27]

$$\text{CWT}_x(a, b) = \frac{1}{\sqrt{a}} \int_{\mathbb{R}} x(t) \psi^* \left(\frac{t-b}{a} \right) dt \quad (9)$$

where $\psi^*(t)$ denotes the complex conjugate of $\psi(t)$, $a \in \mathbb{R}^+$, and $b \in \mathbb{R}$. Equation (9) can also be written as

$$\text{CWT}_x(a, b) = \langle \psi_{a,b}(t), x(t) \rangle \quad (10)$$

where

$$\psi_{a,b}(t) = \frac{1}{\sqrt{a}} \psi \left(\frac{t-b}{a} \right) \quad (11)$$

and the factor $1/\sqrt{a}$ is used to conserve the norm. Thus, (9) measures the similarity between the signal $x(t)$ and shifts and scales of an elementary function. The functions used in the expansion have changing time-frequency tiles because of the scaling. For $a < 1$, $\psi_{a,b}(t)$ will be short and of high frequency. For $a > 1$, $\psi_{a,b}(t)$ will be long and of low frequency. This frequency tiling of wavelet functions is illustrated in Fig. 1(b).

Since the set of basis functions are scaled versions of a single mother wavelet, the term “scale” is often preferred to “frequency” for the CWT. To explore the relationship of scale and resolution in the CWT, we first rewrite (9) as

$$\text{CWT}_x(a, b) = \sqrt{a} \int_{\mathbb{R}} x(at) \psi^* \left(t - \frac{b}{a} \right) dt. \quad (12)$$

Recall that if a function $f(t)$ is scaled in time by a factor of $a > 0$, then it becomes $f(at)$. Scaling in time means that the function is contracted if $a > 1$ and expanded if $a < 1$. Equation (9) implies that as the scale decreases, the filter impulse response $\psi((t-b)/a)$ dilates in time and takes only long-time behavior into account. Similarly, (12) indicates that as the scale increases, an increasingly contracted version of the signal $x(t)$ is seen through a window of fixed length. Hence, the scale factor a has the same meaning as the scale in maps: large scales mean global views while small scales mean detailed views.

On the other hand, the notion of resolution is linked to the frequency content of a signal. For instance, low-pass filtering a signal keeps its scale but reduces its resolution. Moreover,

changes in the scales of continuous-time signals do not change their resolution whereas this is not true for discrete-time signals. For discrete-time signals, increasing the scale involves downsampling which automatically reduces resolution.

D. Filter Banks and Subband Image Decomposition

In the discrete-time case, two methods were developed independently in the late 1970’s and early 1980’s which lead naturally to discrete-time wavelet transforms, namely *subband coding* [5], [28], [29] and *pyramidal coding* or *multiresolution signal analysis* [14]–[16]. Both methods were developed for coding purposes and the concept of critical sampling was of importance. In this section, we briefly review filter banks and their application to subband signal decomposition.

Consider the two-channel filter bank structure shown in Fig. 2, where a discrete-time signal $x(n)$ is applied to a system consisting of a pair of filter banks. Given this original sequence $x(n)$ and its corresponding z -transform $X(z) = \mathcal{Z}\{x(n)\}$, we can obtain a lower-resolution signal by low-pass filtering with a half-band low-pass filter having impulse response $h_1(n)$ with z -transform $H_1(z)$. Then we can make the half-band signal full-band again by downsampling by a factor of two (doubling the scale by a factor of two in the analysis). The z -transform $Y_1(z)$ of the resulting signal $y_1(n)$ can be expressed as

$$Y_1(z) = \frac{1}{2} \left[H_1(z^{1/2})X(z^{1/2}) + H_1(-z^{1/2})X(-z^{1/2}) \right]. \quad (13)$$

Compared with the original sequence $x(n)$, the filtered sequence $y_1(n)$ is reduced in resolution by a factor of two due to half-band low-pass filtering, and doubled in scale, due to downsampling by a factor of two. We can proceed in a similar fashion to compute the “added detail” of the signal as a high-pass filtered version of $x(n)$ using a filter with impulse response $h_2(n)$ and z -transform $H_2(z)$, followed by downsampling by a factor of two as depicted in the lower branch in Fig. 2. The z -transform of $y_2(n)$ can be expressed as

$$Y_2(z) = \frac{1}{2} \left[H_2(z^{1/2})X(z^{1/2}) + H_2(-z^{1/2})X(-z^{1/2}) \right]. \quad (14)$$

At the receiver end of Fig. 2, the filters $g_1(n)$ and $g_2(n)$ are used to reconstruct the signal $\hat{x}(n)$. The inputs to these filters are the decomposed signals $\hat{y}_1(n)$ and $\hat{y}_2(n)$, respectively. Let $\hat{Y}_1(z)$ and $\hat{Y}_2(z)$ be the z -transform of $\hat{y}_1(n)$ and $\hat{y}_2(n)$, respectively. Since by upsampling $\hat{Y}_1(z)$ and $\hat{Y}_2(z)$ we obtain

$\hat{Y}_1(z^2)$ and $\hat{Y}_2(z^2)$, the output of the system can be expressed as

$$\hat{X}(z) = G_1(z)\hat{Y}_1(z^2) + G_2(z)\hat{Y}_2(z^2) \quad (15)$$

where $G_1(z)$ and $G_2(z)$ denote the z -transform of the filters $g_1(n)$ and $g_2(n)$.

If we assume that the encoder-decoder and the channel are error free, that is, if $\hat{Y}_1(z) = Y_1(z)$ and $\hat{Y}_2(z) = Y_2(z)$, then the output becomes

$$\begin{aligned} \hat{X}(z) &= G_1(z)Y_1(z^2) + G_2(z)Y_2(z^2) \\ &= \frac{1}{2}[H_1(z)G_1(z) + H_2(z)G_2(z)]X(z) \\ &\quad + \frac{1}{2}[H_1(-z)G_1(z) + H_2(-z)G_2(z)]X(-z). \end{aligned} \quad (16)$$

The original signal $X(z)$ can be reconstructed by eliminating the term of (16) which involves $X(-z)$. This can be accomplished by requiring that $G_1(z) = 2H_1(z)$, $G_2(z) = -2H_2(z)$ and $H_2(z) = H_1(-z)$. Under these assumptions, (16) becomes

$$\hat{X}(z) = [H_1^2(z) - H_2^2(z)]X(z). \quad (17)$$

The original signal can be perfectly reconstructed if $\hat{x}(n) = x(n)$ or, equivalently, if $\hat{X}(z) = X(z)$. According to (17), perfect reconstruction of the original signal is guaranteed if

$$H_1^2(z) - H_2^2(z) = 1. \quad (18)$$

For simplicity, let $h_1(n) = h(n)$. Then the z -transform of $h_1(n)$ is

$$H_1(z) = \sum_{n=-\infty}^{+\infty} h_1(n)z^{-n} = \sum_{n=-\infty}^{+\infty} h(n)z^{-n}. \quad (19)$$

Since $H_2(z) = H_1(-z)$

$$\begin{aligned} \sum_{n=-\infty}^{+\infty} h_2(n)z^{-n} &= \sum_{n=-\infty}^{+\infty} h(n)(-z)^{-n} \\ &= \sum_{n=-\infty}^{+\infty} (-1)^n h(n)z^{-n} \end{aligned} \quad (20)$$

which implies that

$$h_2(n) = (-1)^n h(n) + (-1)^n h_1(n). \quad (21)$$

This filter equation indicates that if $h_1(n) = h(n)$ is a low-pass filter, then $h_2(n) = (-1)^n h(n)$ is a high-pass filter. The relationship between these two filters becomes obvious by determining the Fourier transform of $h_2(n)$. Since $H_1(\omega) = H(\omega)$, we get

$$\begin{aligned} H_2(\omega) &= \sum_{n=-\infty}^{+\infty} h_2(n)e^{-j\omega n} \\ &= \sum_{n=-\infty}^{+\infty} h(n)(-1)^n e^{-j\omega n} \\ &= \sum_{n=-\infty}^{+\infty} h(n)e^{-j(\omega-\pi)n} \\ &= H(\omega - \pi). \end{aligned} \quad (22)$$

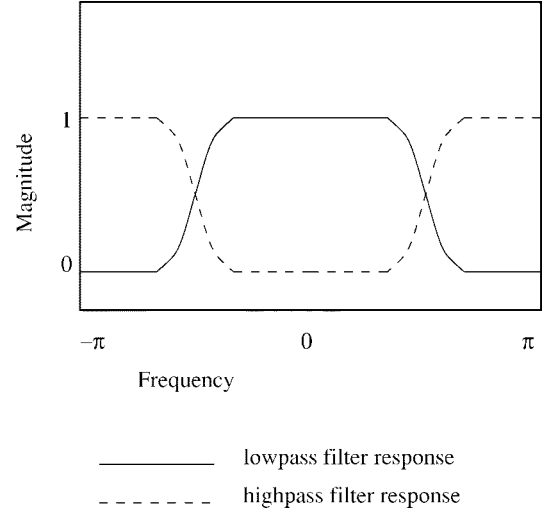


Fig. 3. Frequency response of QMF's; each filter is a half-band filter.

If $h(n)$ is a linear-phase *finite impulse response* (FIR) filter with an even number of coefficients, then the perfect reconstruction condition (18) holds if

$$|H(\omega)|^2 + |H(\omega - \pi)|^2 = 1. \quad (23)$$

Filters that meet the above constraints are said to possess perfect reconstruction properties and are often called *quadrature mirror filters* (QMF's) or *conjugate mirror filters* (CMF's). Fig. 3 shows the magnitude of the frequency response of such filters.

The above results were proposed by Crochiere *et al.* [5] as a means to canceling aliasing in a two-channel filter bank. Even though this solution ensures perfect reconstruction of a signal without aliasing, the design of filters that meet these requirements is a very difficult task and it has been a problem for decades. Fortunately, wavelets can be used to construct FIR filters with perfect reconstruction properties.

E. Wavelet Representation of Images

Wavelet-based image decomposition can be interpreted as an image filtering process. For a given image \mathbf{A} of size $2^n \times 2^n$, wavelet-based subband decomposition can be performed as follows: The wavelet filters $h_1(n)$ and $h_2(n)$ are applied to the rows of the image \mathbf{A} . The filter $h_1(n)$ is a low-pass filter with frequency response $H_1(\omega)$ and $h_2(n)$ is a high-pass filter with frequency response $H_2(\omega)$. By filtering the image \mathbf{A} with $H_1(\omega)$, we obtain low-frequency information (background). By filtering the image with $H_2(\omega)$, we obtain the high-frequency information (edges). After downsampling by a factor of two, we obtain two subbands: $H_{1r}\mathbf{A}$ and $H_{2r}\mathbf{A}$ (the subscript r suggests that the filters are applied to rows of the image \mathbf{A}). Since we downsample by a factor of two in the horizontal direction of each subband, the size of these two downsampled subbands is $2^n \times 2^{n-1}$ (see Fig. 4). The filters $H_1(\omega)$ and $H_2(\omega)$ are then applied to the columns of the subbands $H_{1r}\mathbf{A}$ and $H_{2r}\mathbf{A}$, followed by downsampling by a factor of two, and the following four subbands are obtained: $H_{1c}H_{1r}\mathbf{A}$, $H_{2c}H_{1r}\mathbf{A}$, $H_{1c}H_{2r}\mathbf{A}$, and $H_{2c}H_{2r}\mathbf{A}$. Since we now downsample by a factor of two in the vertical direction of each subband, the four subbands have gone

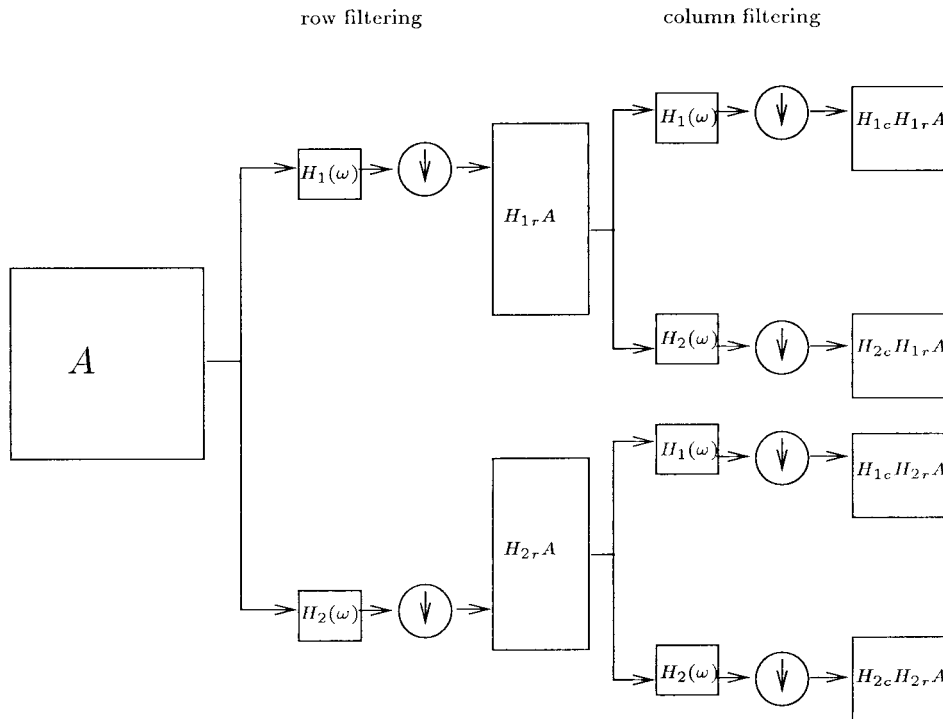


Fig. 4. One level of a two-dimensional subband decomposition using wavelet functions as the analysis filter.

through downsampling by a factor of two in both directions and the final size of each subband is $2^{n-1} \times 2^{n-1}$ (see Fig. 4).

The subband $H_{1c}H_{1r}A$ contains the smooth information and the background intensity of the image and the subbands $H_{1c}H_{1r}A$, $H_{2c}H_{1r}A$, and $H_{1c}H_{2r}A$ contain the detail information of the image. The subband $H_{1c}H_{1r}A$ corresponds to the lowest frequencies, $H_{1c}H_{2r}A$ gives the horizontal high frequencies (vertical edges), $H_{2c}H_{1r}A$ gives the vertical high frequencies (horizontal edges), and $H_{2c}H_{2r}A$ the high frequencies in both directions (corners and diagonal edges).

IV. SYSTEM DESCRIPTION

Screening of digital mammograms for clusters of microcalcifications indicating malignancy can be facilitated by a system capable of extracting spurious spots in digital mammograms regardless of the density of the tissue. This section presents the structure of a system proposed to perform this task by exploiting the frequency selectivity of wavelet-based subband image decomposition.

A. Enhancement and Detection of Spikes

Consider the two-channel filter bank shown in Fig. 2. Under the conditions summarized in Section III-D, this filter bank can be used to perform one level of signal decomposition and reconstruction. Suppose that the signal $x(n)$ is reconstructed by arbitrarily setting $\hat{y}_1(n) = 0, \forall n \in \mathbb{Z}$, which implies that $\hat{Y}_1(z) = 0$. If $\hat{Y}_2(z) = Y_2(z)$, the z -transform of the reconstructed signal $\hat{x}(n)$ can be obtained from (15) as

$$\begin{aligned} \hat{X}(z) &= G_2(z)Y_2(z^2) \\ &= \frac{1}{2}G_2(z)[H_2(z)X(z) + H_2(-z)X(-z)]. \end{aligned} \quad (24)$$

Since $G_2(z) = -2H_2(z)$, (24) gives

$$\hat{X}(z) = -H_2(z)[H_2(z)X(z) + H_2(-z)X(-z)]. \quad (25)$$

Let $x_h(n)$ be the signal produced by passing the original signal $x(n)$ through the high-pass filter with impulse response $h_2(n)$. If $X_h(z)$ denotes the z -transform of $x_h(n)$, then

$$X_h(z) = H_2(z)X(z) \quad (26)$$

and

$$X_h(-z) = H_2(-z)X(-z). \quad (27)$$

Thus, (25) can also be written as

$$\hat{X}(z) = -H_2(z)[X_h(z) + X_h(-z)]. \quad (28)$$

Since $\mathcal{Z}^{-1}\{X_h(-z)\} = (-1)^n x_h(n)$, (28) implies that

$$\hat{x}(n) = h_2(n) * x_{hh}(n) \quad (29)$$

where $*$ denotes the convolution operator and

$$\begin{aligned} x_{hh}(n) &= -[1 + (-1)^n]x_h(n) \\ &= \begin{cases} -2x_h(n), & \text{if } n \text{ is even} \\ 0, & \text{if } n \text{ is odd.} \end{cases} \end{aligned} \quad (30)$$

In other words, the reconstructed signal $\hat{x}(n)$ is produced by passing the signal $x_{hh}(n)$ defined at (30) through the high-pass filter with impulse response $h_2(n)$.

The signal $x_h(n)$ is obtained by passing the original signal $x(n)$ through a high-pass filter. High-pass filtering of the original signal $x(n)$ tends to suppress its homogeneous portions and enhance the existing discontinuities and spikes. The signal $x_{hh}(n)$ is obtained by multiplying the amplitude of the samples by -2 and replacing every second sample

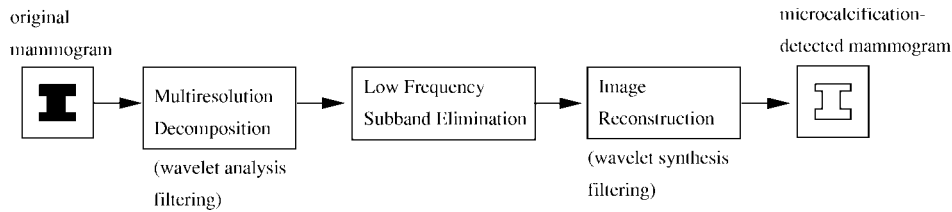


Fig. 5. The proposed system in operation: the input to the system is a digital mammogram; the output is a mammogram with detected microcalcifications.

by zero. This guarantees that spikes will be preserved in the signal $x_{hh}(n)$ provided that their duration is larger than one sample. The addition of zeros creates abrupt transitions from one sample to the next and tends to introduce additional high frequencies to the signal $x_{hh}(n)$. High-pass filtering of $x_{hh}(n)$ will further enhance the discontinuities and spikes present. This analysis indicates that the discontinuities and spikes present in the original signal $x(n)$ can be enhanced and detected by setting the subband carrying the lowest frequencies to zero. The condition for spike detection is that the resolution of the discrete-time signal is sufficiently high so that the duration of each spike is larger than one sample.

Image decomposition is performed by independently applying filtering and downsampling to the rows and columns of the image. Thus, the results of the above analysis can naturally be extended to images. In other words, spikes and abrupt intensity level changes in images can be enhanced and detected by setting the subband carrying the lowest frequencies to zero. Such an approach can be used to enhance and detect microcalcifications in mammograms provided that they occupy an area larger than a window of size 2×2 pixels. The performance of such a system would be affected by the resolution of the digital mammograms and the behavior of the filters used to perform image decomposition. Due to high-pass filtering, this approach is not immune to “noisy spikes” or other artifacts. The elimination of “noisy spikes” and artifacts can only be accomplished by preprocessing or postprocessing procedures.

B. The Proposed System

The system proposed for microcalcification detection is based on the hypothesis that the microcalcifications present in mammograms can be preserved under a transform which can localize the signal characteristics in the original and the transform domain. In a time signal the harmonic frequency components are present but they are *hidden*, whereas in its frequency spectrum the time information is *hidden*. Therefore, transforms with basis functions other than the complex sinusoids must be used. In addition, these basis functions must be able to localize the signal in both spatial and frequency domains. A suitable transform that satisfies the above requirements is the *wavelet transform*. The wavelet transform uses basis functions that can *dilate* in scale and *translate* in position according to the signal characteristics [9].

Given that the microcalcifications correspond to high-frequency components of the image spectrum and wavelets can localize the signal characteristics in both frequency and scale, our hypothesis is that the resolution and scale of the

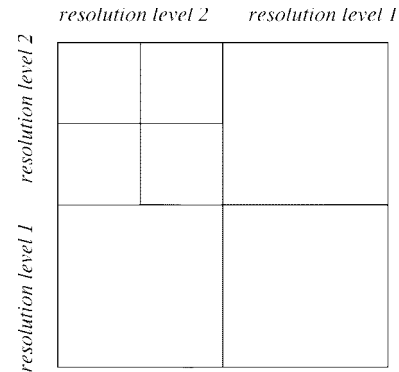


Fig. 6. Orthogonal subbands at different resolutions produced by two levels of wavelet decomposition of a 512×512 image.

microcalcifications in the spatial domain can be preserved if we use wavelet filters to decompose the mammogram into different frequency subbands. According to this hypothesis, microcalcifications can be extracted from mammograms by suppressing the subband of the wavelet-decomposed image that carries the lowest frequencies and contains smooth (background) information, before the reconstruction of the image.

The proposed system is described in the block diagram shown in Fig. 5. The original mammogram is decomposed into a set of orthogonal subbands of different resolution and frequency content. The decomposition is based on wavelet analysis filtering and downsampling along the rows and columns of the image. Fig. 6 shows the seven subbands resulting after two levels of wavelet decomposition of a 512×512 image. The four subbands at resolution 1 are produced by the decomposition scheme described in Section III-E. The application of the same decomposition scheme to the upper-left subband that carries the lowest frequencies at resolution 1 results in the two-level subband decomposition shown in Fig. 6. In the wavelet-decomposed image shown in Fig. 6, the upper-left subband at resolution level 2 contains the background intensity of the original image and, thus, carries the lowest frequencies of the image spectrum. The microcalcifications, which correspond to the highest frequencies, are carried by the other subbands. The detection of microcalcifications is accomplished by setting the wavelet coefficients of the upper-left subband to zero in order to suppress the image background information before the reconstruction of the image. The reconstructed mammogram is expected to contain only high-frequency components, including the microcalcifications. The final images are obtained using subband reconstruction, which is the inverse operator of subband decomposition. The reconstruction consists of wavelet

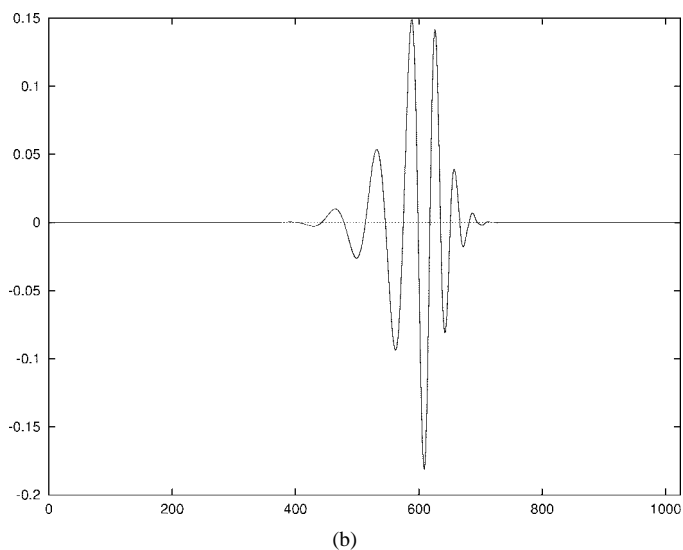
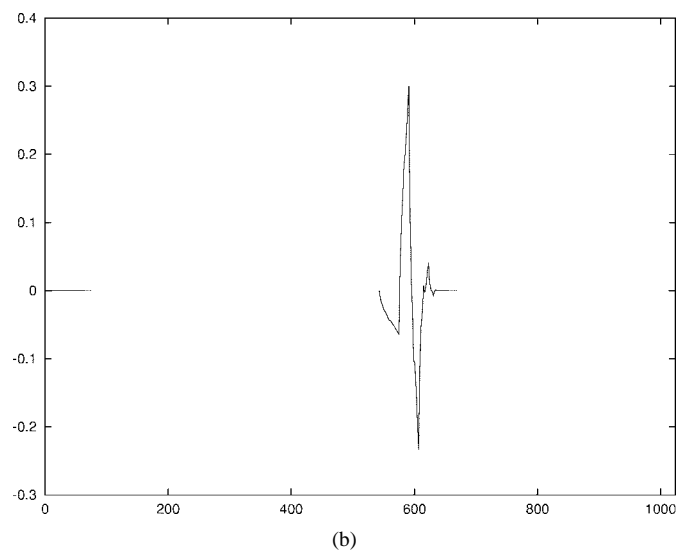
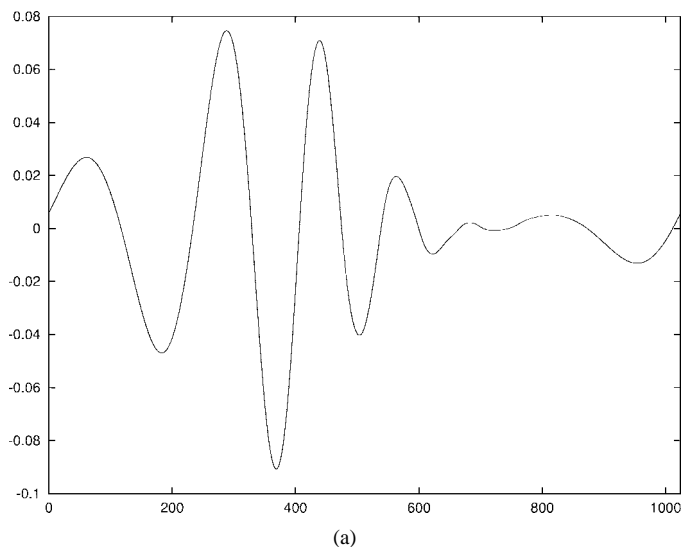
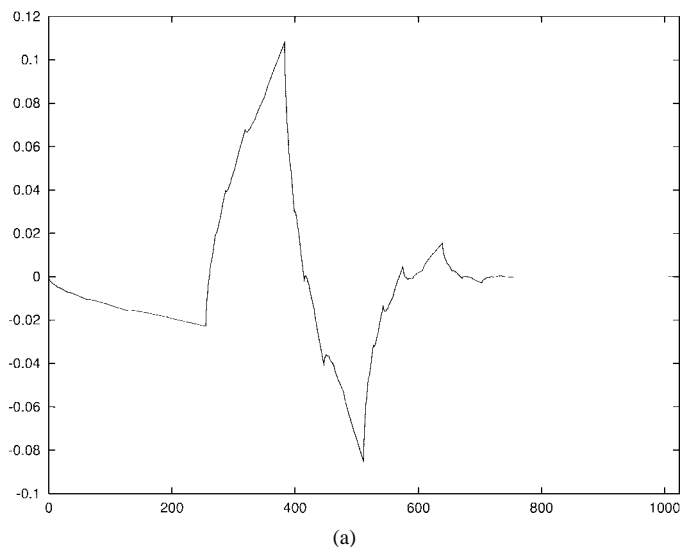


Fig. 7. The mother wavelet ψ of the DAUB 4 wavelets: (a) a wide and short wavelet for analyzing low-frequency characteristics and (b) a narrow and tall wavelet for analyzing high-frequency characteristics.

Fig. 8. The mother wavelet ψ of the DAUB 20 wavelets: (a) a wide and short wavelet for analyzing low-frequency characteristics and (b) a narrow and tall wavelet for analyzing high-frequency characteristics.

synthesis filtering and upsampling along the rows and columns of the image.

The visibility of microcalcifications is improved by using a nonlinear thresholding method to enhance the histogram of the resulting mammograms. More specifically, the input dynamic range of a mammogram is initially determined. Given the input range, the image is transformed through a nonlinear mapping based on the arc-tangent method. This nonlinear thresholding method is designed to improve the visibility of microcalcifications by increasing their pixel intensity relative to their background.

C. Wavelet Filters

In the “wavelet analysis filtering” and “wavelet synthesis filtering” stages, we have used the so-called “maximally flat” wavelet filters constructed by Daubechies [7]. These wavelets are *compactly supported* and *regular*. Wavelets are compactly supported if they have finite support with maximum number of vanishing moments for their support width.

Compact support improves the time resolution of wavelets. Regularity relates to differentiability. Since differentiation in Fourier domain amounts to a multiplication by $(j\omega)$, existence of derivatives is related to sufficient decay of the Fourier spectrum.

Table I shows the filter coefficients of the two wavelets from Daubechies’ family of orthonormal wavelets used in this paper, namely the Daubechies’ 4-coefficient (DAUB 4) filter and Daubechies’ 20-coefficient (DAUB 20) filter [7]. Fig. 7 shows the amplitude plot of the mother wavelet ψ for the family of DAUB 4 filters. Fig. 7(a) represents the “long window” used to analyze long-term behavior of a signal; whereas Fig. 7(b) is the scaled and translated version of the same wavelet used to analyze the instantaneous behavior of a signal. Fig. 8 shows the amplitude plot of the mother wavelet ψ for the family of DAUB 20 filters. In each case, note that the stretched wavelets have higher amplitudes while the dilated wavelets have lower amplitudes, in concordance with the constant- Q requirement described in Section III-C.

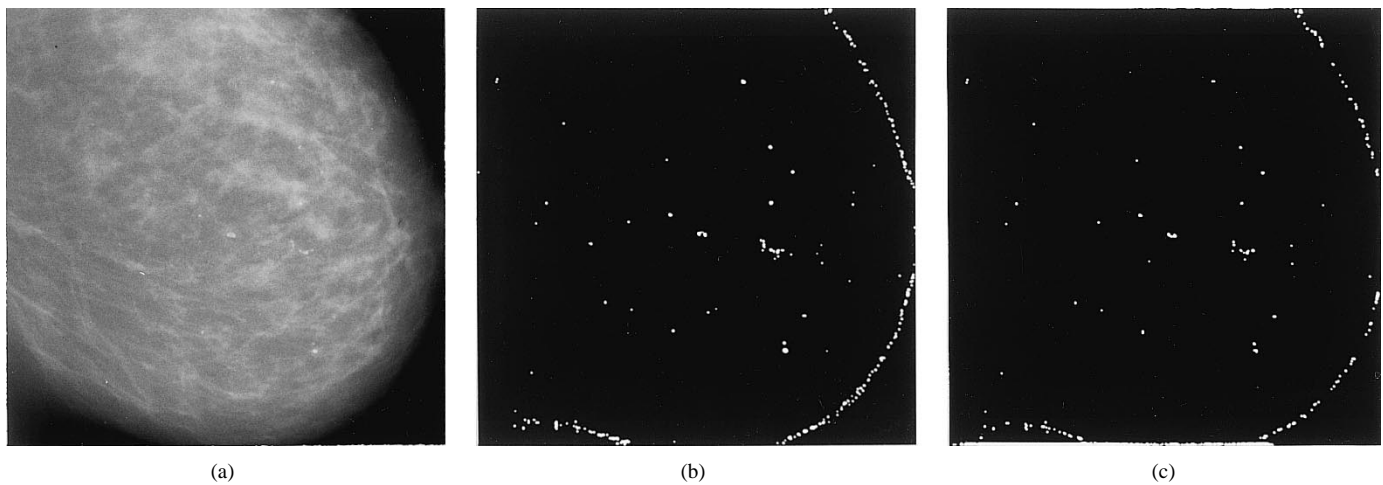


Fig. 9. (a) The original mammogram. Microcalcifications extracted from the original mammogram decomposed using (b) the DAUB 4 filter and (c) the DAUB 20 filter.

TABLE I
COEFFICIENTS OF THE DAUB 4 AND DAUB 20 FILTERS. GIVEN THE
LOW-PASS FILTER $g_0(n)$, THE HIGH-PASS FILTER CAN BE OBTAINED AS
 $g_1(n) = (-1)^n g_0(-n + 2N - 1)$, WHERE N IS THE LENGTH OF THE FILTER

	DAUB 4	DAUB 20
n	$g_0(n)$	$g_0(n)$
0	0.482691	0.026670
1	0.836516	0.188177
2	0.224143	0.527207
3	-0.129409	0.688459
4		0.281172
5		-0.249846
6		-0.195946
7		0.127369
8		0.093057
9		-0.071394
10		-0.029457
11		0.033212
12		0.003606
13		-0.010733
14		0.001395
15		0.001992
16		-0.000686
17		-0.000116
18		0.000093
19		-0.000013

D. An Example

The preliminary testing of the proposed system was based on the digital mammogram shown in Fig. 9(a). Fig. 9(b) and (c) shows the images obtained after processing the original mammogram using the DAUB 4 and DAUB 20 filters, respectively. All microcalcifications present in the original mammogram are visible in the images produced by the proposed system, which also traced the boundary of the breast in the original mammogram. The performance of the proposed

system depends on the length of the wavelet filters used in the decomposition of the mammograms. This is a direct consequence of the different shapes of the corresponding mother wavelets. According to Figs. 7 and 8, the mother wavelet of the DAUB 4 filter is more “spike-like” compared with that of the smoother DAUB 20 filter. It is clear from these images that the DAUB 4 filter detects more pixels of high spatial frequency compared with the DAUB 20 filter. These pixels may belong to microcalcifications, breast boundary, or background noise. Thus, shorter wavelet filters are more sensitive to existing microcalcifications but they tend to produce more false positives.

V. CONCLUSIONS

Previous studies suggested that wavelet-based image analysis techniques could occupy a leading position in digital mammography [13]. The proposed approach to microcalcification detection was motivated by the ability of wavelets to discriminate different frequencies and to preserve signal details at different resolutions. In fact, this approach exploits the orientation and frequency selectivity of the wavelet transform to make the microcalcifications more visible. This method is robust in the sense that it does not require the use of heuristics or the prior knowledge of the size and the resolution of the mammogram. All this is due to the “zoom in” and “zoom out” capability of the wavelet filters which can *translate* themselves to a location of a signal that is of interest and *dilate* themselves properly to preserve the resolution of that portion of the signal. The preliminary experiments presented in this paper indicate that further studies are needed to investigate the potential of wavelet-based subband image decomposition as a tool for microcalcification detection. These studies must investigate how the performance of this approach is affected by: 1) the properties of the wavelet filters used for subband image decomposition, 2) the intensity contrast between the background and breast tissue, 3) the resolution of the original digital mammogram, and 4) artifacts present in the original mammogram. Additional studies must also include *receiver operating characteristic* analysis to account for the effect of the threshold on false positive and false negative rates.

ACKNOWLEDGMENT

The authors would like to thank S. S. Pinero, M.D., a radiologist with extensive experience in mammography, for providing her valuable advice on various aspects of clinical mammography.

REFERENCES

- [1] G. T. Barnes and G. D. Frey, Eds., *Screen Film Mammography. Imaging Considerations and Medical Physics Responsibilities*. Madison, WI: Med. Phys., 1991.
- [2] J. J. Benedetto and M. W. Frazier, *Wavelets: Mathematics and Applications*. Boca Raton, FL: CRC, 1994.
- [3] D. Betal, "Extraction of microcalcifications from digital mammograms using mathematical morphology," in *Proc. Inst. Elect. Eng. Colloquium on Morphological and Nonlinear Image Processing Techniques*, 1993, pp. 9/1–3.
- [4] A. Y. Cairns, I. W. Ricketts, D. Folkes, M. Nimmo, P. E. Preece, A. Thompson, and C. Walker, "The automated detection of clusters of microcalcifications," in *Proc. Inst. Elect. Eng. Colloquium on Applications of Image Processing in Mass Health Screening*, 1982, pp. 3/1–5.
- [5] R. E. Crochiere, S. A. Webber, and J. L. Flanagan, "Digital coding of speech in subbands," *Bell Syst. Tech. J.*, vol. 55, no. 8, pp. 1069–1085, 1976.
- [6] I. Daubechies, "Orthonormal bases of compactly supported wavelets," *Commun. Pure and Appl. Math.*, vol. 41, pp. 909–996, 1988.
- [7] ———, *Ten Lectures on Wavelets*. Philadelphia, PA: SIAM, 1992.
- [8] J. Dengler, S. Behrens, and J. Desaga, "Segmentation of microcalcifications in mammograms," *IEEE Trans. Med. Imag.*, vol. 12, pp. 634–642, Aug. 1993.
- [9] M. Farge, J. C. R. Hunt, and J. C. Vassilicos, *Wavelets, Fractals, and Fourier Transforms*. New York, NY: Oxford Univ. Press, 1993.
- [10] D. Gabor, "Theory of communications," *J. Inst. Elect. Eng.*, vol. 93, pp. 429–457, 1946.
- [11] P. C. Johns and M. J. Yaffe, "X-ray characterization of normal and neoplastic breast tissues," *Phys. Med., Biol.*, vol. 32, no. 6, pp. 675–695, 1987.
- [12] S. Lai, X. Li, and W. Bischof, "On techniques for detecting circumscribed masses in mammograms," *IEEE Trans. Med. Imag.*, vol. 8, pp. 377–386, Aug. 1989.
- [13] A. F. Laine, S. Schuler, J. Fan, and W. Huda, "Mammographic feature enhancement by multiscale analysis," *IEEE Trans. Med. Imag.*, vol. 13, pp. 725–740, Aug. 1994.
- [14] S. G. Mallat, "A theory for multiresolution signal decomposition: The wavelet representation," *IEEE Trans. Pattern Anal. Machine Intell.*, vol. 11, pp. 674–693, July 1989.
- [15] ———, "Multiresolution approximations and wavelet orthonormal bases of $L^2(\mathbb{R})$," *Trans. Amer. Math. Soc.*, vol. 315, no. 1, pp. 69–87, 1989.
- [16] ———, "Multifrequency channel decomposition of images and wavelet models," *IEEE Trans. Acoust., Speech, Signal Processing*, vol. 37, pp. 2091–2110, Dec. 1989.
- [17] F. Mintzer, "Filters for distortion-free two-band multirate filter banks," *IEEE Trans. Acoust., Speech, Signal Processing*, vol. 33, pp. 626–630, Mar. 1985.
- [18] W. Morrow, R. Paranjape, R. Rangayyan, and J. Desautels, "Region-based contrast enhancement of mammograms," *IEEE Trans. Med. Imag.*, vol. 11, pp. 392–406, June 1992.
- [19] R. M. Nishikawa, Y. Jiang, M. L. Giger, K. Doi, C. J. Vyborny, and R. A. Schmidt, "Computer-aided detection of clustered microcalcifications," in *Proc. IEEE Int. Conf. Syst., Man, Cybern.*, 1992, pp. 1375–1378.
- [20] M. J. T. Smith and T. P. Barnwell, III, "Exact reconstruction for tree-structured subband coders," *IEEE Trans. Acoust., Speech, Signal Processing*, vol. 34, pp. 431–441, Mar. 1986.
- [21] R. A. Smith, "Epidemiology of breast cancer," in *A Categorical Course in Physics. Technical Aspects of Breast Imaging*, A. G. Haus and M. J. Yaffe, Eds. Oak Brook, IL: Radiological Soc. No. Amer., 1993, pp. 119–135.
- [22] P. P. Vaidyanathan, "Theory and design of M -channel maximally decimated quadrature mirror filters with arbitrary M , having the perfect reconstruction property," *IEEE Trans. Acoust., Speech, Signal Processing*, vol. 35, pp. 476–492, Apr. 1987.
- [23] ———, "Quadrature mirror filter banks, M -band extensions and perfect reconstruction techniques," *IEEE Trans. Acoust., Speech, Signal Processing Mag.*, vol. 4, no. 3, pp. 4–20, 1987.
- [24] M. Vetterli, "Filter banks allowing perfect reconstruction," *Signal Processing Mag.*, vol. 10, no. 3, pp. 219–244, 1986.
- [25] M. Vetterli and D. LeGall, "Perfect reconstruction FIR filter banks: Some properties and factorizations," *IEEE Trans. Acoust., Speech, Signal Processing*, vol. 37, pp. 1057–1071, July 1989.
- [26] M. Vetterli and C. Herley, "Wavelets and filter banks: Theory and design," *IEEE Trans. Signal Processing*, vol. 40, pp. 2207–2232, Sept. 1992.
- [27] M. Vetterli and J. Kovacevic, *Wavelets and Subband Coding*. Englewood Cliffs, NJ: Prentice-Hall, 1995.
- [28] P. H. Westerink, D. E. Boekee, J. Biemond, and J. W. Woods, "Subband coding of images using vector quantization," *IEEE Trans. Commun.*, vol. 36, no. 6, pp. 713–719, 1988.
- [29] J. W. Woods and S. D. O'Neil, "Subband coding of images," *IEEE Trans. Acoust., Speech, Signal Processing*, vol. 34, no. 5, pp. 1278–1288, 1986.
- [30] M. J. Yaffe, R. J. Jennings, R. Fahrig, and T. R. Fewell, "X-ray spectral considerations for mammography," in *A Categorical Course in Physics: Technical Aspects of Breast Imaging*, A. G. Haus and M. J. Yaffe, Eds. Oak Brook, IL: Radiological Soc. No. Amer., 1993, pp. 63–72.
- [31] D. Zhao, M. Shridhar, and D. G. Daut, "Morphology on detection of calcifications in mammograms," in *Proc. IEEE Int. Conf. Acoustics, Speech, and Signal Processing*, San Francisco, CA, Mar. 1992, pp. 129–132.